Critical roles of ICOS in controlling Foxp3-expressing T follicular cell subsets during early-stage germinal center reactions

Vincent Panneton [1,2], Barbara C. Mindt [3,4], Yasser Bouklouch [1], Jinsam Chang [1,5], Mariko Witalis [1,5], Joanna Li [1,3], Albert Stancescu [1], Antoine Bouchard [1,5], John E. Bradley [6], Troy D. Randall [6], Jörg H. Fritz [3,4], Woong-Kyung Suh [1, 2, 3, 5, *]

[1] Institut de Recherches Cliniques de Montréal (IRCM), Quebec, Canada.
[2] Department of Microbiology, Infectiology and Immunology, University of Montreal, Quebec, Canada.
[3] Department of Microbiology and Immunology, McGill University, Quebec, Canada.
[4] McGill University Research Centre on Complex Traits (MRCCT), McGill University, Quebec, Canada.
[5] Molecular Biology Program, University of Montreal, Quebec, Canada.
[6] Department of Medicine, Division of Clinical Immunology and Rheumatology, University of Alabama at Birmingham, Alabama, United States.

* Correspondence: Woong-Kyung Suh, Institut de Recherches Cliniques de Montréal (IRCM), 110 av. des Pins Ouest, Montréal, Québec, Canada.

Email: woong-kyung.suh@ircm.qc.ca

Author contributions

V.P. and W-K.S. conceived and supervised the study. V.P., B.C.M., Y.B., J.C., M.W., J.L. and A.S. performed the experiments. V.P., Y.B., A.B. and W-K.S. analyzed the data. J.E.B., T.D.R. and J.H.F. contributed key reagents and resources. V.P. and W-K.S. wrote the manuscript. V.P., B.C.M., Y.B., M.W., J.L., A.B. and W-K.S. commented and revised the manuscript.

ABSTRACT

The inducible costimulator (ICOS) is a T cell costimulatory receptor critical for humoral immunity. In mice and humans, ICOS deficiency leads to a lack of T follicular helper (Tfh) cells and protective antibodies. However, the role of ICOS in T follicular regulatory (Tfr) cell generation and function remains poorly understood. Using Foxp3-cre-mediated ICOS knockout (ICOS FC) mice, we show that T regulatory (Treg)-specific ICOS deletion drastically reduces the number of Tfr cells without altering Treg cell numbers. Further, we observed a lowered ratio of antigen-specific germinal center B (GC B) cells and increased anti-nuclear antibodies in ICOS FC mice, suggesting a rise of autoreactive GC B cells. Single-cell transcriptome analysis revealed shifts in transitory Tfr precursor populations in immunized ICOS FC mice. Mechanistically, our data suggest that ICOS promotes the Treg-to-Tfr transition by regulating KLF2 and NFAT2 with downstream impacts on Bcl6 and CXCR5 expression. Importantly, we discovered a Tfr subset originating from Foxp3^{-} precursors by analyzing flow cytometry data of immunized mice in which ICOS expression in Foxp3^{+} cells was ablated at different stages of GC reactions. Consistently, single-cell transcriptome analysis of global follicular T cells revealed a subset of Tfh-like cells beginning to express Foxp3 at day 6 post-immunization. These “Tfh-like Tfr” cells appear to promote GC B cell expansion and plasma cell differentiation in an ICOS-dependent manner. Taken together, we propose that Tfr cells derived from natural Tregs suppress the expansion of autoreactive GC B cells whereas “Tfh-like Tfr” cells promote early-stage GC output. Further, these Tfr subsets depend on ICOS costimulation for their differentiation or function.

Introduction

High affinity class-switched antibodies are essential for immune responses against pathogens. These antibodies arise from germinal centers (GCs) where T follicular helper (Tfh) cells facilitate the transition of GC B cells into antibody-secreting plasma cells (PCs) [1,2]. Tfh cells are defined by combined expression of their master transcription factor Bcl6 along with CXCR5, PD-1 and ICOS [3-6]. Tfh cells mediate their helper functions through costimulation by CD40L and ICOS along with the production of the cytokines IL-4 and IL-21 [7-9]. Because dysregulation of Tfh cells and GC reactions can lead to humoral autoimmunity, they must be tightly controlled [10].

T follicular regulatory (Tfr) cells are a subset of $CD4^+$ $Foxp3^+$ regulatory T (Treg) cells found in and around germinal centers [11-14]. Like Tfh cells, they express the chemokine receptor CXCR5 which is required for their migration towards B cell follicles [11-13]. The transcription factor NFAT2 was recently shown to be required for CXCR5 upregulation by Tfrs, possibly to overcome BLIMP-1-mediated CXCR5 downregulation [15-17]. There are no known lineage-defining factors specific to Tfr cells, although they require concomitant expression of Foxp3 and Bcl6 [18,19]. A significant proportion of Tfr cells originate from thymic Tregs and possess a T cell receptor (TCR) repertoire skewed towards self-antigens [11-13,20]. Under specific conditions, induced Tregs have displayed the capacity to differentiate into Tfr cells that can be specific for the immunizing antigen [21]. Strong IL-2 signaling was shown to inhibit Tfr differentiation which is more akin to Tfh cells rather than Tregs [22]. Interestingly, recent reports provide evidence that Tfh cells can also give rise to Tfr-like cells [23,24]. While the *in vivo* role of Tfr cells has been controversial, they display suppressive abilities on T cell proliferation, antibody secretion and cytokine

production *in vitro* [25,26]. Several Tfr depletion models have been studied to understand their functions *in vivo*. Initially, adoptive transfer or mixed bone marrow (BM) chimera experiments showed that Tfr reduction had varying effects on GC responses, possibly due to unintended side effects such as impaired Treg function [11-13]. More recently, Foxp3-specific deletion of Bcl6-expressing (Bcl6 FC) or CXCR5-expressing cells (Tfr-deleter) allowed for a more precise assessment of *in vivo* roles for Tfr cells [19,27-30]. Results from these studies collectively suggest two roles for Tfr cells: suppression of autoantibody production and modulation of antibody responses more suggestive of "helper" functions [31].

The inducible costimulator (ICOS) is a member of the CD28 superfamily and is known to be expressed by activated T cells [32]. ICOS was previously shown to be essential for the formation of Tfh cells and maintenance of Bcl6 expression [33-35]. In both mice and humans, ICOS null mutations cause severe defects in GC reactions and antibody production driven by lack of Tfh cells [36-39]. Some ICOS-deficient patients develop autoimmune symptoms such as rheumatoid arthritis and autoimmune neutropenia, suggesting a potential role for ICOS in Treg/Tfr compartments [40,41]. Indeed, ICOS deficiency in mice led to reduced Tfr cell numbers, although the underlying mechanisms have not been carefully analyzed [26,42].

In this study, we used *Icos*$^{fl/fl}$ *Foxp3-cre* (ICOS FC) and *Icos*$^{fl/fl}$ *Foxp3-cre*^{ERT2} (ICOS FCERT2) mice to evaluate the role of ICOS signaling in Treg and Tfr cells during GC reactions. Foxp3-specific loss of ICOS led to a significant decrease of Tfr populations after protein immunization or viral infection without affecting Treg cell numbers in ICOS FC mice. Examination of antibody responses revealed significantly lowered IgG2b titers

at steady state or after immune challenge along with increased anti-nuclear autoantibodies in ICOS FC mice. Single-cell transcriptomics and biochemical analyses suggest that ICOS may enhance the Treg-to-Tfr transition through KLF2 and NFAT2 regulation. Inducible Foxp3-specific ICOS abrogation revealed that part of the Tfr compartment originates from Foxp3^{-} cells and can increase GC output in an ICOS-dependent manner. Overall, our findings indicate that ICOS can selectively impact the differentiation or function of different Tfr compartments in early-stage GC reactions and highlight the importance of Tfr cells in regulating GC output while preventing autoantibody generation.

RESULTS

ICOS is required for Tfr cell generation during GC reactions against protein antigens

To assess the role of ICOS in Treg lineage cells, we used a Foxp3-cre system which allows for the specific abrogation of ICOS expression in all Treg and Tfr cells. Throughout this study, we used *Icos*$^{+/+}$ *Foxp3-cre*$^{+}$ controls (ICOS WT) for *Icos*$^{fl/fl}$ *Foxp3-cre*$^{+}$ mice (ICOS FC). First, we analyzed splenocytes 12 days after immunization with NP-OVA/alum by flow cytometry and subdivided the CD4^{+} Foxp3^{+} regulatory T cell compartment into Treg (CD4^{+} Foxp3^{+} CXCR5^{-} PD-1^{-}), PD-1^{-} Tfr (CD4^{+} Foxp3^{+} CXCR5^{+} PD-1^{-}) and PD-1^{+} Tfr (CD4^{+} Foxp3^{+} CXCR5^{-} PD-1^{+}) subsets (Fig. 1a). ICOS was expressed in both Tfh (CD4^{+} Foxp3^{-} CXCR5^{+} PD-1^{+}) and Treg/Tfr cells, with PD-1^{+} Tfr cells showing the highest surface levels (Supplementary Fig. 1a).

We confirmed that ICOS deletion was limited to Foxp3^{+} cells and did not occur in Tfh cells (Supplementary Fig. 1b). We observed no change of total Foxp3^{+} populations in ICOS FC mice (Fig. 1a). However, we found ~2-fold and ~4-fold decreases in PD-1^{-} and PD-1^{+} Tfr cell proportions and numbers, respectively. Interestingly, these reduced Tfr populations were balanced by an increased proportion of Treg cells. Next, we examined Tfh, GC B cells and plasma cells since lack of Tfr cells has been shown to increase these populations in some experimental settings [11-13]. We did not observe significant differences in Tfh cell proportion or absolute numbers (Fig. 1a). We also detected no quantitative differences in GC B cell and plasma cell populations (Fig. 1b-c). Consistently, NP-specific IgG1 antibodies in serum did not show changes in total (NP30) or high affinity (NP7) titers (Fig. 1d). Taken together, these results indicate that loss of ICOS in Foxp3^{+} cells leads to

a reduced number of Tfr cells with proportionally increased Treg cells, suggesting an impaired Treg-to-Tfr transition.

ICOS is required for Tfr generation during anti-viral response

To evaluate the role of ICOS in regulatory T cell compartments during an anti-viral immune response, we infected mice with influenza A virus (IAV). We analyzed splenocytes by flow cytometry 30 days after infection since it has been shown that Tfr generation is delayed due to high levels of IL-2 present in the early stages of viral infection [22]. We observed an increased proportion of Tregs and decreases in Tfr populations in spleens of ICOS FC mice reminiscent of results from protein immunization experiments (Fig. 2a). As before, we did not detect significant differences in Tfh populations (Fig. 2b). To exclude the possibility that ICOS only modifies CXCR5 expression levels measured by flow cytometry without affecting Tfr cells, we used the essential Tfr transcription factor Bcl6 as an alternative Tfr marker and confirmed significant Tfr decreases in ICOS FC mice (Supplementary Fig. 2). Next, we examined the expansion of GC B cell populations that recognize the IAV nucleoprotein using recombinant tetramers (Flu tetramer) [43]. Interestingly, we observed a trend of increased total GC B cells with a significantly decreased proportion of IAV-specific GC B cells in ICOS FC mice (Fig 2c). This results in a significant increase of extraneous GC B cells, some of which could be autoreactive in nature. On the other hand, we did not observe significant differences in splenic plasma cells (Fig. 2d). However, we found significant decreases of IAV-specific IgG2b serum titers (Fig. 2e). Consistent with the role of anti-viral antibodies in the overall control of influenza virus [44], we observed that ICOS FC mice had more severe weight loss 9-10

days post-infection (Supplementary Fig. 3a). This reduced anti-viral IgG2b titer was well correlated with a reduction of total IgG2b titers in infected ICOS FC mice (Supplementary Fig. 3b). Further, we noticed that uninfected ICOS FC mice had decreased basal levels of IgG2b and IgG1 (Supplementary Fig. 3c), suggesting that ICOS-expressing Treg or Tfr cells may work as “helper” T cells for certain antibody isotype switching. Thus, congruent with data from protein immunization experiments, this infection model confirmed the critical role of ICOS for efficient Tfr generation. Further, increases of non-viral specific GC B cells in ICOS FC mice confirms the regulatory role of Tfr cells in shaping GC responses.

Treg-specific ICOS deficiency leads to anti-nuclear antibody production

Since there is ongoing cell death and release of autoantigens within the GC, autoreactive GC B cell clones can expand and differentiate into plasma cells with help from Tfh cells if not restrained [10]. Given that Foxp3-specific ICOS ablation results in reduced numbers of Tfr cells which are thought to suppress self-reactive antibody production, we investigated whether ICOS FC mice displayed signs of autoimmunity. We did not observe immune infiltration in the kidneys, lungs, spleen, pancreas, and salivary glands of 5-month-old ICOS FC mice (Fig. 3a). Next, we used HEp-2 slides to look for the presence of anti-nuclear antibodies (ANAs) which are a hallmark of autoimmunity (Fig. 3b) [45]. We did not detect significant spontaneous increases of ANAs in serum samples of 6-month-old ICOS FC mice. However, we found that both single NP-OVA/alum immunization and secondary challenge with the same antigen resulted in significantly higher ANAs in ICOS FC mice. Additionally, ICOS FC mice infected with influenza A virus presented similar increases in ANA levels. These results suggest that immunization or

infection augments adventitious generation of autoantibodies which is normally suppressed by Tfr cells.

ICOS-deficient Treg cells show impaired transition to Tfr cells

To better understand the role of ICOS in Tfr cell differentiation, we performed single-cell transcriptome analysis of $CD4^+$ $Foxp3^+$ splenocytes sorted from ICOS WT and ICOS FC mice immunized with NP-OVA/alum. To collect cells in a dynamic Treg-to-Tfr transition stage, we prepared samples 6 days post-immunization, a timepoint where Tfr cells begin to appear [22,26]. After sorting, we added back sorted conventional $CD4^+$ $Foxp3^-$ T cells (~10% of total) into the sorted $CD4^+$ $Foxp3^+$ T cell pool to provide a reference point (Supplementary Fig. 4a, cluster 4). We used Tfr-defining genes (*Cxcr5, Pdcd1, Foxp3, Bcl6*) to calculate a "Tfr identity score" and selected three clusters that are predicted to contain Tfr precursors and mature Tfr cells (Supplementary Fig. 4b, clusters 3, 5, 8 black arrows). When compared amongst each other, these cells formed three distinct clusters with a spectrum of Tfr identity score (Fig. 4a, clusters 1, 2, 3). Pseudotime trajectory analysis revealed a progressive differentiation from cluster 1 towards cluster 3 (Fig. 4b). Interestingly, we observed that ICOS FC mice presented a 3-fold increase of cells in cluster 2 and a 3-fold decrease in cluster 3 (Fig. 4a). This suggests that Tregs could be halted in their transition to Tfr cells due to loss of ICOS expression. To substantiate this idea, we compared gene expression profiles of the three clusters (Fig. 4c, left). Cluster 3 had the highest levels of key Tfr signature genes (*Cxcr5, Pdcd1, Bcl6*), but reduced expression of typical Treg signature genes such as *Foxp3, Il2ra* (CD25), *Ctla4* and *Tnfrsf18* (GITR) when compared to clusters 1 and 2. However, when compared with $CD4^+$

Foxp3^{-} conventional T cells, cluster 3 still mostly maintained higher levels of these Treg signature genes (Fig 4c, right). Recent studies have identified CD25 downregulation as a key event in Tfr differentiation [22,46]. Similarly, we noticed that CD25 expression is inversely correlated with the levels of CXCR5 and PD-1 in Tfr cells, consistent with a previous report by Wing *et al.* [46] (Supplementary Fig. 5a, b). Congruent with CD25 protein expression levels, *Il2ra* gene expression was significantly dampened in cluster 3 Tfr cells compared to those in clusters 1 and 2 (Fig. 4d). Interestingly, cluster 2 cells from ICOS FC mice displayed significantly higher *Il2ra* levels suggesting that ICOS could be involved in CD25 downregulation. ICOS ablation also resulted in significantly elevated CD25 protein expression in certain Tfr subsets (Supplementary Fig. 5b). Apart from CD25, we noticed a significant decrease of *Tgfb1* expression in ICOS FC cluster 3 cells (Fig. 4e). This could explain reduced IgG2b titers observed in ICOS FC mice since TGF-β1 is a known class switch factor for this isotype [47].

Another key event in the Treg-to-Tfr transition is CXCR5 upregulation [11-13,15]. ICOS was previously shown to regulate CXCR5 by suppressing KLF2 expression in Tfh cells [48]. This mechanism may operate in Treg/Tfr cells since we observed that *Icos* and *Klf2* gene expression is inversely correlated and that all three clusters had higher *Klf2* expression in ICOS FC mice (Fig. 4f). KLF2 was also shown to dampen Tfh differentiation by increasing S1PR1 and BLIMP-1 expression levels [49]. We observed matching expression patterns of *Klf2, S1pr1 and Prdm1* with opposed *Bcl6* expression in all clusters (Fig. 4g). Further, ICOS FC mice showed an accumulation of *Klf2*$^{+}$ *S1pr1*$^{+}$ *Prdm1*$^{+}$ cells in cluster 2 with reduced *Bcl6* expression in clusters 2 and 3. Thus, these results suggest

that ICOS is required for a few key steps in the Treg-to-Tfr transition and that failure of these processes seem to lead to an accumulation of putative Tfr precursors.

ICOS ablation causes decreased NFAT2 activation and impaired CXCR5 expression in Tregs.

To test the potential role of ICOS in upregulating CXCR5 expression, we further analyzed our single-cell transcriptome data. We found that clusters 1 and 2 from ICOS FC mice had lowered proportions of *Cxcr5*$^{+}$ cells along with a diminished average *Cxcr5* expression (Fig. 5a). Next, we investigated the potential impacts of ICOS signaling on NFAT2 (product of *Nfatc1* gene), a transcription factor known to directly bind to the promoter region of C*xcr5* [15]. Importantly, we and others have previously shown that ICOS can potentiate TCR-mediated calcium flux, a key factor in NFAT activation [50,51]. Consistently, we found that the average expression levels of known NFAT target genes (Supplementary Table 1) was significantly decreased in ICOS FC cluster 2 cells when compared to ICOS WT control (Fig. 5b, top). Since Tfr precursor-like cells in cluster 2 also express the highest levels of *Nfatc1* (Fig. 4c), we tested whether *Nfatc1* expression level was reduced in ICOS FC cluster 2 cells. However, we did not find significant differences in the expression level of the *Nfatc1* gene itself (Fig. 5b, bottom). Nonetheless, we noticed that the protein levels of ICOS and NFAT2 trended higher in Tfr cells compared to Treg cells, suggesting a potential role of ICOS-NFAT2 in the Treg-to-Tfr transition (Fig. 5c). Consistent with our single-cell transcriptomics data, we found that both PD-1^{-} and PD-1^{+} Tfr subsets from infected ICOS FC mice displayed significantly decreased CXCR5 expression (Fig. 5d). Congruent with the unaltered *Nfatc1* mRNA levels in ICOS FC Tfr

populations, we found that NFAT2 protein expression levels were not decreased in ICOS-deficient Tfr subsets (Fig. 5e).

Because we observed that ICOS deletion led to decreased expression of NFAT target genes but not NFAT2 itself, we investigated other regulatory mechanisms. It has been established that NFAT2 activity depends on its dynamic nuclear-cytoplasmic shuttling controlled by its phosphorylation status [50]. To evaluate if ICOS can regulate this process, we expanded purified splenic $CD4^+$ T cells *in vitro* and acutely restimulated them through the TCR (CD3) with or without ICOS costimulation. Cytoplasmic and nuclear NFAT2 proteins of varying migration properties were then harvested separately by fractionation and quantified by Western blot (Fig. 5f). Without restimulation, 5-10 min incubation at 37ºC led to the increase of hyperphosphorylated (slower migrating) NFAT2 species in the cytoplasm with concomitant disappearance of hypophosphorylated (faster migrating) NFAT2 species in the nucleus (lanes 1 and 2 in cytoplasmic and nuclear fractions). This is presumably due to temperature-induced shifts in the activity of NFAT phosphatases and kinases [50]. As predicted, CD3 ligation increased NFAT2 nuclear levels (lanes 3 and 4). Importantly, combined CD3/ICOS stimulation further augmented nuclear NFAT2 levels at 10 min when compared with CD3 stimulation alone (Fig. 5g). This increase was dependent on ICOS since it was abolished when ICOS KO $CD4^+$ T cells were used (Fig. 5h). Taken together, our biochemical data shows that ICOS costimulation can potentiate TCR-driven NFAT2 activation in $CD4^+$ T cells. Thus, we propose that ICOS could act upstream of the NFAT2-CXCR5 signaling axis known to be one of the key mechanisms for early Tfr differentiation [15].

Inducible Foxp3-specific ICOS ablation suggests the presence of Foxp3^{-} Tfr precursors and leads to increased GC output in an ICOS-dependent manner.

Foxp3 expression is induced in thymic Tregs early in their development [52]. Since the ICOS FC system is triggered as soon as Foxp3 is expressed, we cannot exclude impacts of ICOS ablation early during Treg development on subsequent Tfr populations. To rule out this possibility, we introduced a Foxp3-specific, tamoxifen-inducible cre system (*Icos$^{fl/fl}$ Foxp3-cre^{ERT2}*, named ICOS FCERT2) which provides temporal control of ICOS depletion. We began by inducing ICOS ablation 5 days prior to immunization with NP-OVA/alum (Fig. 6a). Analysis of splenocytes 12 days post-immunization revealed a two-fold reduction of PD-1^{+} Tfr cells mirrored by a two-fold increase of Tfh cells (Fig. 6 b, c). To understand why these results do not match those obtained using ICOS FC mice, we measured ICOS expression in various T cell subsets to evaluate whether ICOS ablation was successful (Fig. 6d). As expected, ICOS was found to be absent from Treg and PD-1^{-} Tfr cells but preserved in Tfh cells. Unexpectedly, we found a subset of PD-1^{+} Tfr cells with intact ICOS expression levels and low levels of Foxp3 expression (Fig. 6e). This suggests that Foxp3^{-} cells acquired Foxp3 expression after tamoxifen has been cleared, thus giving rise to a Tfr-like population that has escaped ICOS ablation. These findings fit with a recent report showing that Tfh cells can acquire Foxp3 expression at the end-stage of GC reactions [24]. We will henceforth use the term “Tfh-like Tfr” to refer to this population. While the role of the Tfh-like Tfr subset remains unknown in early-stage GCs, we observed a significant increase of GC B cells and plasma cells in the spleen of ICOS FCERT2 mice 12 days post-immunization (Fig. 6 f, g).

To evaluate the role of ICOS in Tfh-like Tfr cells, we delayed Foxp3-specific ICOS ablation to days 7-11 post immunization so that this Tfr subset may acquire Foxp3 expression (Supplementary Fig. 6a). Ablation of ICOS after immunization did not cause further loss of PD-1$^+$ Tfr cells when compared to pre-immunization ICOS abrogation (Supplementary Fig. 6b, c). Since all PD-1$^+$ Tfr cells from ICOS FCERT2 mice lose ICOS expression when tamoxifen treatment is performed after immunization, this suggests that ICOS may not be required for Tfh-like Tfr differentiation or survival (Supplementary Fig. 6d). Interestingly, Foxp3-specific ICOS abrogation post-immunization did not cause increases of Tfh, GC B cell and plasma cell populations which suggests a functional requirement of ICOS for Tfh-like Tfr cells (Supplementary Fig. 6c, e, f). Thus, we propose that a subset of Tfr cells originate from Foxp3$^-$ precursors and can lead to increased GC output in an ICOS-dependent manner.

Single cell transcriptome analysis of follicular T cells from early-stage GCs reveals three distinct Tfr cell subsets.

To gain better insight into the composition of Tfr cell compartments, we performed single-cell transcriptome analysis of CD4$^+$ CXCR5$^+$ PD-1$^+$ follicular T cells isolated from the spleen of a normal C57BL/6 mouse 6 days post-immunization with NP-OVA/alum. Using Foxp3 expression levels, we defined clusters of Foxp3$^+$ and Foxp3$^-$ follicular T cells as well as a hybrid cluster (Fig. 7a, b). Next, we created three distinct Tfr-like signatures based on shared expression of key genes (Supplementary Table 2). Signatures of GC Tfr cells and Treg-like Tfr cells were defined based on data from our regulatory T cell transcriptome analysis (Fig. 4). For the Tfh-like Tfr signature, we used the most

upregulated genes from the Foxp3 hybrid cluster (Fig. 7a). Applying these newly defined Tfr-like signatures on the cluster map revealed three distinct populations with only partial overlap (Fig. 7c). Additionally, we applied these signatures to the total cluster map generated from our regulatory T cell transcriptome analysis and observed no notable overlap of the three Tfr-like populations (Fig. 7d). Interestingly, the relative abundance and number of cells in the Tfh-like Tfr cluster did not decrease in ICOS FC mice which supports the view that these cells do not require ICOS for their differentiation or survival (Fig. 7e). In sum, our single cell transcriptome analysis identified three distinct Tfr-like populations that are present in early-stage germinal centers. Further, our data suggests that, unlike GC Tfr cells, Tfh-like Tfr cells can arise in the absence of ICOS.

Discussion

In this study, we identified ICOS as a critical costimulatory receptor for Tfr differentiation and function upon immune challenges. We showed that Foxp3-specific ICOS ablation in ICOS FC mice results in altered gene expression patterns at the single-cell level leading to an accumulation of Tfr precursor-like cells and a substantial reduction of the fully differentiated "GC Tfr" population. Further, ICOS FC mice displayed an increase of extraneous GC B cells without increases of total GC B cell or Tfh cell numbers. ICOS FC mice also showed an elevated incidence of autoantibody production after GC reactions, presumably due to an expansion of autoreactive B cells. In contrast, total and virus-specific IgG2b antibody titers under steady-state and upon influenza infection were diminished in ICOS FC mice. Our single-cell data strongly suggests that ICOS-mediated downregulation of KLF2 plays a key role in shaping chemokine receptor expression and balancing BLIMP-1-Bcl6 levels in developing Tfr cells. Our biochemical analysis demonstrates that ICOS signaling can also augment NFAT2 nuclear localization, potentially counterbalancing the negative impacts of BLIMP-1 on CXCR5 expression [15,16].

Our single-cell RNA transcriptome analysis of Foxp3$^+$ cells from ICOS WT and ICOS FC mice indicates that dynamic changes in gene expression patterns drive the Treg-to-Tfr transition. Trajectory analysis reveals that the CD25$^+$ BLIMP-1$^+$ activated Treg subset progressively gains follicular features such as CXCR5 and Bcl6. Both single-cell transcriptomics and flow cytometry data demonstrate that Bcl6 and CXCR5 levels are highest in CD25$^-$ "GC-Tfr" cells, the main Foxp3$^+$ cells shown to be found within the GC [46]. During this Treg-to-Tfr transition, ICOS seems to utilize a mechanism that has been shown to be critical for the differentiation and maintenance of Tfh cells – timely

downregulation of KLF2 [49]. As such, Tfr precursor cells reduced levels of *Klf2* and its main target genes *S1pr1* and *Prdm1* along the predicted Tfr trajectory. In contrast, *Cxcr5* and *Bcl6* expression levels were progressively elevated in cells that have dampened *Klf2* target genes, presumably due to the lack of BLIMP-1-mediated suppression of Bcl6. Importantly, this progression towards "GC-Tfr" was halted at the *Klf2*^{hi} *Prdm1*^{hi} stage in ICOS-deficient Treg cells. Therefore, we propose that ICOS-mediated KLF2 downregulation is a key molecular event that initiates follicular T cell programing in Tfr cells.

In addition to KLF2, ICOS may utilize NFAT2-dependent pathways to support CXCR5 expression during the Treg-to-Tfr transition. Although NFAT2 is highly expressed in both Tfh and Tfr cells, abrogation of NFAT2 expression in T cells was shown to cause more pronounced defects in Tfr generation as opposed to Tfh differentiation due to compromised CXCR5 expression [15]. This observation fits well with the idea that developing Tfr cells need higher concentrations of nuclear NFAT2 to overcome elevated levels of BLIMP-1 (known repressor of *Cxcr5* gene [16]) that are present in Tfr precursor cells. Our biochemical data indicate that ICOS ligation augments the amount of nuclear NFAT2 in TCR-activated CD4^{+} T cells. Based on these, we speculate that ICOS costimulation reinforces CXCR5 expression in early Treg-derived Tfr precursors leading to the establishment of "GC-Tfr" differentiation.

While we showed that ICOS signaling can maintain NFAT2 in the nucleus, the mechanism remains unclear. Nuclear transport of NFAT family members occurs through their dephosphorylation by calcineurin, a Ca^{2+} dependent phosphatase [50]. We have previously shown that ICOS signaling can potentiate TCR-induced intracellular Ca^{2+} flux,

although we did not determine if this resulted in increased NFAT activity [51]. Conversely, nuclear export of NFAT2 is triggered by phosphorylation through several kinases including GSK3β [53]. In turn, GSK3β activity can be inhibited by Akt-mediated phosphorylation of residue Ser9 [54]. We and others have shown that ICOS stimulation can increase PI3K/Akt signaling, specifically through its Y^{181}MFM cytoplasmic tail motif [35,55,56]. Thus, we suggest that ICOS could maintain NFAT2 nuclear localization by increasing its import through enhanced Ca^{2+} signaling and/or decrease its export by inhibiting GSK3β.

Apart from its role in facilitating Treg-to-Tfr transitions, ICOS seems to be involved in controlling overall GC output – a contentious role for Tfr cells [31]. Contrary to the prevailing view that almost all Tfr cells arise from thymic Tregs, our single-cell transcriptome analysis of total follicular T cells indicates that a substantial number of Tfh-like Tfr cells arise during normal GC reactions as early as six days post immunization. Through acute ICOS gene ablation experiments, we observed $Foxp3^{-}$ $CD4^{+}$ T cells gain Foxp3 expression while maintaining high levels of ICOS, CXCR5, and PD-1 implying a Tfh-to-Tfr conversion. Unlike Treg-derived Tfr cells, this Tfh-like Tfr population is sustained in the absence of ICOS. However, its putative functions – facilitation of GC B cell expansion and plasma cell differentiation appear to be ICOS-dependent.

The fact that a portion of mature Tfh cells can acquire Foxp3 expression has been recently confirmed by Jacobsen *et al.* [24]. However, the authors observed this population arising in end-stage germinal centers up to 20 days post-immunization. Although data suggests that these Foxp3-expressing Tfh cells may terminate GC reactions, the fate of GC B cells has not been addressed. In comparison, we detected Tfh-like Tfr cells as early as day 6 post-immunization, and they seem to increase GC B cell expansion and

differentiation. More work is needed to clarify whether these two populations represent different waves of Tfh-derived Tfr cells with potentially diverging roles.

We speculate that our Tfh-like Tfr cells arise from Tfh cells after encountering GC B cells that have undergone some level of affinity maturation. Once formed, Tfh-like Tfr cells may expedite expansion of GC B cells and their differentiation into short-lived plasma cells through ICOS-dependent T-B conjugation [57]. In an infection scenario, this may help control the spreading of pathogens during a period when unmutated antibodies generated through extrafollicular reactions decline while high-affinity long-lived humoral immunity is yet to be established.

The biological roles of Tfr cells during GC reactions remain ill-defined. Tfr depletion studies using Bcl6 FC mice have shown small decreases of antibodies specific for the immunizing antigen [19,58,59]. One study also showed spontaneous increases of autoantibodies and multi-organ lymphocytic infiltration in aged mice [28]. Along the same line, high levels of anti-nuclear antibodies were generated in Bcl6 FC mice after influenza infection [22]. ICOS FC mice do not display age-related autoantibodies or lymphocytic infiltrations, suggesting that the impact of ICOS-deficiency on Treg cells is weaker than that of Bcl6-deficiency. In this context, Bcl6-deficient Treg cells (as opposed to bona-fide Tfr cells) could have contributed to some of these phenotypes considering recent reports that Bcl6-deficient Tregs have compromised suppressive functions in other immune settings [60-62]. ICOS deficiency was shown to impair the suppressive ability of Tregs in asthma and type 1 diabetes murine models, but no defects in GC reactions were reported [63,64]. Combined with a ~4-fold reduction in the Tfr number, it seems likely that humoral immune defects in ICOS FC mice are mainly due to reduced Tfr numbers. Another

potential role for Tfr cells is to promote the generation of antigen-specific antibodies. Bcl6 FC mice produce reduced amounts of IgE and IgG1 in certain immunization protocols [58,59]. We found that both basal IgG2b (in unimmunized mice) and anti-influenza IgG2b titers are lower in ICOS FC mice. This correlated well with reduced amounts of TGF-β1 mRNA in the GC-Tfr population. However, further work is required to clarify the mechanisms and biological implications of this finding.

In sum, we showed that ICOS is critically important for Tfr differentiation and function. In Treg-derived Tfr cells, ICOS-mediated downregulation of KLF2 and its target genes can shape the Bcl6-driven Tfr programming whereas an ICOS-NFAT2-CXCR5 signaling axis may reinforce CXCR5 expression during Treg-to-Tfr transitions. On the other hand, Foxp3^{-} T cell-derived Tfr populations can be maintained without ICOS but may be functionally impaired. Our work identifies distinct Tfr populations arising from two different origins and provides a conceptual framework for future studies

Figure legends

Figure 1. Foxp3-specific ICOS ablation decreases Tfr populations in a protein immunization model.

Splenocytes from ICOS WT (n=5) and ICOS FC (n=4) mice were harvested 12 days post-immunization (dpi) with NP-OVA/alum and analyzed by flow cytometry. (A) Treg, Tfr and Tfh cell percentages and numbers were evaluated using a combination of Foxp3, PD-1 and CXCR5 staining. (B) $B220^+$ Fas^+ $GL7^+$ GC B cell populations and (C) $B220^-$ $CD138^+$ plasma cells populations were analyzed from the same splenocyte pool 12 dpi. (D) Total (NP30) and high affinity (NP7) anti-NP IgG1 titers were measured by ELISA using serum from ICOS WT (black, n=5) or ICOS FC mice (red, n=5) obtained 28 dpi. Data shown as mean ± SEM, *p<0.05, **p<0.01, ***p<0.001. All data are representative of at least three independent experiments.

Figure 2. ICOS FC mice display reduced Tfr populations along with increased extraneous GC B cells during anti-viral responses.

Splenocytes from ICOS WT (n=5) or ICOS FC (n=4) were harvested 30 days post-infection (dpi) with influenza A virus (IAV) and analyzed by flow cytometry. (A) $Foxp3^+$ Treg and Tfr cells were classified using CXCR5 and PD-1 staining. (B) $Foxp3^-$ $CXCR5^+$ $PD\text{-}1^+$ Tfh cells were analyzed from the same splenocyte pool. (C) $B220^+$ Fas^+ $GL7^+$ GC B cells were harvested from spleens 30 dpi and stained with influenza nucleoprotein-specific tetramers (flu tetramers). (D) $B220^-$ $CD138^+$ plasma cells were analyzed using the same splenocyte pool. (E) IAV-specific IgG1, IgG2b and IgG2c titers were measured by ELISA using serum samples from ICOS WT (black) and ICOS FC mice (red) obtained 30 dpi. Data shown as mean ± SEM, *p<0.05, **p<0.01, ***p<0.001. All data are representative of two independent experiments.

Figure 3. ICOS FC mice produce increased anti-nuclear antibodies following immune challenge.

(A) Representative images of H&E-stained tissue sections from 5-month-old ICOS WT (n=3) and ICOS FC mice (n=3). Scale bar 200 µM. (B) Anti-nuclear antibodies were detected by staining HEp-2 slides with serum samples collected from mice after the following treatments. Unimmunized ICOS WT (n=4) and ICOS FC (n=6) mice at 6 months of age. Primary immunization of ICOS WT (n=5) and ICOS FC (n=5) mice with NP-OVA/alum (serum harvested 12 dpi). Secondary NP-OVA/alum injection 30 days after the primary injection (serum harvested 44 days post secondary challenge). IAV infection of ICOS WT (n=5) and ICOS FC (n=5) mice (serum harvested 30 dpi). Scale bar 50µM. Nuclear fluorescence intensity was quantified using ImageJ. Data shown as mean ± SEM, *p<0.05. All data are representative of two independent experiments.

Figure 4. ICOS-deficient Treg cells show impaired Treg to Tfr transition.

Single-cell transcriptomes of FACS-sorted $CD4^+$ $Foxp3^+$ splenocytes from an ICOS WT or ICOS FC mouse harvested 6 days after protein immunization. (A) Selection and sub-clustering of $Foxp3^+$ cells based on positive Tfr identity scores. (B) Pseudotime analysis showing the differentiation trajectory of selected $Foxp3^+$ splenocytes. (C) Mean expression of regulatory and follicular genes by the indicated subpopulation. (D) *Il2ra* (E) *Tgfb1*, (F) *Icos* and *Klf2* violin plots showing the gene expression levels subdivided by cluster identities defined in (A). (G) Feature plots of *Klf2, S1pr1, Prdm1* and *Bcl6* expression. Each dot represents one cell. *p<0.05, **p<0.01, ***p<0.001.

Figure 5. ICOS-NFAT2 signaling may regulate CXCR5 expression in regulatory T cells.

(A) Feature plot of *Cxcr5* gene expression (top) and quantification of *Cxcr5*$^+$ cells along with average *Cxcr5* expression in clusters 1 & 2 cells (bottom). (B) Average expression of NFAT target genes (top) and expression of *Nfatc1* (bottom) subdivided by cluster identity. (C) Splenocytes from ICOS WT (n=5) and ICOS FC mice (n=7) were analyzed 30 dpi with IAV. ICOS and NFAT2 expression was compared in Treg, PD-1^- Tfr and PD-

1^+ Tfr cells coming from ICOS WT mice. (D) MFI values for CXCR5 in PD-1^- Tfr and PD-1^+ Tfr cells from the same splenocyte pool. (E) NFAT2 MFI values in ICOS WT vs. ICOS FC Treg, PD-1^- Tfr and PD-1^+ Tfr cells were measured using the same splenocyte pool. (F) ICOS WT and ICOS germline KO $CD4^+$ T cells were isolated from spleens by magnetic sorting and cultured for 2 days with α-CD3/CD28 stimulation. Cells were then restimulated for the indicated times with combinations of isotype control, α-CD3 and α-ICOS antibodies after which cytoplasmic and nuclear fractions were extracted and analyzed for NFAT2 protein content by Western blot. (G) Bar graph representing normalized cytoplasmic vs. nuclear NFAT2 band quantification of the indicated samples at the 10min timepoint. Only the bottom NFAT2 band was quantified to represent hypophosphorylated nuclear NFAT2. (H) Normalized nuclear NFAT2 band intensity of α-CD3/α-ICOS stimulated samples from ICOS WT vs. KO cells at 10 min. Data shown as mean ± SEM, *p<0.05, **p<0.01, ***p<0.001. All data are representative of two independent experiments.

Figure 6. Inducible Foxp3-specific ICOS ablation reveals $Foxp3^-$ Tfr precursors and leads to increased GC output

(A) ICOS WT (n=5) and ICOS FCERT2 (n=4) mice were treated with tamoxifen once per day for 5 days before immunization with NP-OVA/alum. Splenocytes were harvested 12 dpi. (B) Flow cytometry gating strategy for Treg, Tfr, and Tfh compartments. (C) Treg, Tfr and Tfh cell percentages and numbers were evaluated using a combination of CD4, Foxp3, PD-1 and CXCR5 staining. (D) ICOS expression in the indicated compartment, blue histograms represent ICOS WT mice and red histograms represent ICOS FCERT2 mice. (E) Foxp3 expression in $ICOS^-$ PD-1^+ Tfr vs. $ICOS^+$ PD-1^+ Tfr subsets from ICOS FCERT2 mice. (F) $B220^+$ Fas^+ $GL7^+$ GC B cell populations and (G) $B220^-$ $CD138^+$ plasma cells populations were analyzed from the same splenocyte pool. Data shown as mean ± SEM, *p<0.05, **p<0.01, ***p<0.001. All data are representative of at least three independent experiments.

Figure 7. Single cell transcriptome analysis of follicular T cells identifies three distinct Tfr subsets

(A) Single-cell transcriptomes of FACS-sorted $CD4^+$ $CXCR5^+$ $PD\text{-}1^+$ splenocytes harvested 6 days after protein immunization classified based on *Foxp3* expression. (B) Feature plots of the indicated genes using clustering defined in panel A. (C) Subclustering of Tfr cells based on signatures defined in supplementary table 2. (D) Signatures defined in panel C were applied to single-cell transcriptome data from ICOS WT and ICOS FC mice represented in supplementary figure 4. (E) Relative abundance and number of cells in the Tfh-like Tfr clusters from ICOS WT and ICOS FC mice defined in panel D.

Methods

Mice and animal procedures

C57BL/6, *Foxp3*$^{YFP\text{-}Cre}$ mice (Jax 016959) [65], and Foxp3$^{EGFP\text{-}CreERT2}$ (Jax 016961) [66] were purchased from the Jackson Laboratory. ICOS conditional knockout mice were generated in C57BL/6 background as previously described [67]. ICOS germline knockout mice have been backcrossed onto C57BL/6 background for more than ten generations [36]. All mice were housed in the Institut de Recherches Cliniques de Montréal animal care facility under specific pathogen-free conditions. Animal experiments were performed in accordance with animal use protocols approved by the Institut de Recherches Cliniques de Montréal Animal Care Committee. All mice were 8-12 weeks of age unless specified otherwise. For protein immunization, mice were injected intraperitoneally with 100 µg of 4-Hydroxy-3-nitrophenylacetyl hapten-17 (NP17)-OVA (Biosearch Technologies, 1 µg/mL) mixed with Imject Alum (ThermoFisher) in a 1:1 ratio. For viral infections, mice were infected intranasally with a sublethal dose of influenza A virus H1N1 (strain A/Puerto Rico/8/34 (PR8), 10 PFU/20g body weight). For tamoxifen gavage, mice were fed orally with 10 µL/g of 20 mg/mL tamoxifen (Millipore Sigma) dissolved in corn oil (Millipore Sigma) once per day for 5 consecutive days.

Flow cytometry

For analysis, single-cell suspensions were prepared by mechanical disruption of spleens unless specified otherwise. Viability was assessed by staining $1x10^8$ cells/mL with fixable viability dye eFluor 780 (ThermoFisher) for 20 mins at 4ºC. Fc receptors were blocked using anti-CD16/CD32 (BioXCell). For intracellular staining, cells were fixed and

permeabilized using the Transcription Factor Staining Buffer Set (ThermoFisher). Surface or intracellular staining was performed at $1x10^8$ cells/mL for 20 mins at 4ºC. The following antibodies were used. BD Biosciences: anti-CD4 BUV395 (GK1.5), anti-PD-1 BV421 (RMP1-30), anti-CD95 PE-Cy7 (Jo2), anti-Bcl6 PE (K112-91). ThermoFisher: anti-B220 PerCP-eFluor 710 (RA3-6B2), anti-CXCR5 Biotin (SPRCL5), Streptavidin PE-Cy7, anti-ICOS FITC (7E.17G9), anti-Foxp3 APC (FJK-16s), anti-B220 eFluor 450 (RA3-6B2), anti-CD25 PE (PC61.5). BioLegend: anti-NFATc1 PE (7A6), anti-GL7 FITC (GL7). To identify influenza-specific B cells, we used tetramerized recombinant nucleoproteins conjugated with APC or PE (Flu tetramer) provided by Dr. Troy Randall [43]. Data was acquired using a BD LSRFortessa and analyzed using FlowJo v10 (BD Biosciences).

ELISA

Serum samples were obtained from blood collected from the submandibular vein at the indicated timepoints. Plates were coated with either goat anti-mouse IgG (SouthernBiotech), NP30-BSA and NP7-BSA (Biosearch Technologies), or heat-inactivated influenza A viruses overnight at 4ºC. Serum samples underwent a 2-fold serial dilution starting from the indicated initial dilution. Bound antibodies were detected using alkaline phosphatase-conjugated anti-IgG1/2b/2c/3, IgM or IgA and *p*-nitrophenyl phosphate substrate (SouthernBiotech). The reaction was stopped by adding 1.5 N NaOH solution and optical density was measured at 405 nm.

Histology

Organs were dissected and fixed in 10% neutral buffered formalin for 12 h at 4ºC. Organs were then washed in 1x PBS, embedded in paraffin, and cut into 5 µM sections. Slides were stained with H&E to examine immune cell infiltration of organs.

Anti-nuclear antibody assay

Serum samples were obtained from blood collected from the submandibular vein at the indicated timepoints and incubated on Kallestad HEp-2 slides (Bio-Rad) according to the manufacturer's instructions. Bound antibodies were detected using goat anti-mouse IgG Alexa Fluor 555 (ThermoFisher). Fluorophore signals were visualized using a DMRB fluorescence microscope (Leica). Nuclear MFI was quantified using ImageJ.

Single-cell RNA sequencing

For Foxp3^{+} cell transcriptome analysis, splenocytes from *Foxp3*$^{YFP\text{-}cre}$*Icos*$^{+/+}$ (ICOS WT) and *Foxp3*$^{YFP\text{-}cre}$*Icos*$^{fl/fl}$ (ICOS FC) male mice were isolated 6 dpi with NP-OVA/alum and stained with anti-CD4 Alexa Fluor 647 (GK1.5, BioLegend), anti-TCRβ PE-Cy7 (H57-597, BioLegend) and propidium iodide (ThermoFisher). Live (PI^{-}) conventional (YFP^{-}) and regulatory (YFP^{+}) CD4^{+}TCRβ^{+} T cells were sorted with a BD FACSAria (BD Biosciences) to >95% purity. Sorted conventional and regulatory T cells were mixed in a 1:10 ratio to provide an internal control. A total of 13500 cells from ICOS WT and ICOS FC mice were sent for library preparation. For follicular T cell transcriptome analysis, splenocytes from *a* normal C57BL/6 (*Stk4*$^{+/-}$ used as control for other experiments) mouse were isolated 6 dpi with NP-OVA/alum and stained with anti-CD4 Alexa Fluor 647 (GK1.5, BioLegend),

anti-CXCR5 Biotin (SPRCL5) & Streptavidin PE-Cy7 (ThermoFisher), anti-PD-1 BV421 (RMP1-30, BD Biosciences) and propidium iodide (ThermoFisher). Live (PI^-) conventional ($CD4^+CXCR5^-PD\text{-}1^-$) and follicular ($CD4^+CXCR5^+PD\text{-}1^+$) T cells were sorted with a BD FACSAria (BD Biosciences) to >95% purity. Sorted conventional and follicular T cells were mixed in a 1:10 ratio to provide an internal control. A total of 15000 cells were sent for library preparation. Libraries were generated using the following components from 10x Genomics: Chromium Next GEM Chip G Single Cell kit, Chromium Next GEM Single Cell 3' GEM, Library & Gel Bead kit v3.1, Chromium i7 Multiplex kit. Sequencing was performed by Genome Québec using a NovaSeq 6000 (Illumina) with a flow cell S1 PE28*91.

Reads alignment

Using *Cellranger* 4.0.0 (from *10xGenomics*®), we generated a custom reference genome using the GRCm38.p6 (mm10) assembly procured from *Ensembl* to which we added the *Ires-Yfp-iCre* sequence as described in its design map [65]. The alignment of the reads was performed using the same software and the resulting expression matrix was loaded into *R* version 3.6.1 (from the R Foundation for Statistical Computing) to conduct analysis.

Single cell expression matrix analysis

The expression matrices were stored into an R Seurat object available in the package *Seurat* version 3.0 [68] to ease the analysis. ICOS WT and ICOS FC samples were merged during the filtering phase which consisted of the elimination of any cell that presented more than 10% mitochondrial RNA contamination as well as any cell with less than 200 unique genes expressed. The expression matrix was then log normalized and

scaled. We identified the most differentially expressed genes within the samples and proceeded with a dimensional reduction using a principal component analysis (PCA) approach based on the 2000 most variable features. We selected the first 30 most important eigenvectors produced by the PCA to construct a *Shared Nearest Neighbor* (SNN) graph and used *Modularity Optimizer version 1.3.0* [69] to identify 13 clusters. The cells were projected on a 2D space using a *Uniform Manifold Approximation and Projection UMAP* method [70]. We isolated 3 clusters of interest based on their markers and moved the normalized expression matrix into an R *cell_data_set* object available in the package *Monocle3* version 0.2.3 [71]. Using the dimensionally reduced matrices of expression, a differentiation trajectory was constructed. The cells were then ordered along the trajectory and pseudotime was computed. We further confirmed the consistency of our trajectory analysis using a diffusion map-based approach (available in package *destiny* version 2.0.4) which has proven to be more robust to noise [72]. We computed NFAT signaling gene expression score using the *AddModuleScore* function available in the *R* library *Seurat v3.0*. The list of NFAT target genes was established using the PANTHER classification system combined with data from literature and can be found in Supplementary table 1 [15,73-75]. Tfr subcluster signatures are based on expression of genes listed in Supplementary table 2.

$CD4^+$ T cell activation and Western blot analysis

$CD4^+$ T cells were isolated from spleens and lymph nodes using the EasySep mouse $CD4^+$ T cell isolation kit (StemCell Technologies) according to the manufacturer's instructions. Purified T cells were stimulated from 2 days in complete RPMI 1640 (10%

FBS, 1 unit/mL penicillin, 1 µg/mL streptomycin, 55mM β-mercaptoethanol and 10 mM HEPES) with plate-bound anti-CD3 (BioXCell, 3 µg/mL) and soluble anti-CD28 (ThermoFisher, 2 µg/mL). For restimulation, $CD4^+$ T cell blasts were incubated for 3 mins at room temperature with the indicated combination of the following antibodies: 1 µg/mL Armenian hamster IgG isotype control (BioXCell), 1 µg/mL anti-CD3e (145-2C11, ThermoFisher) and 2 µg/mL anti-ICOS (C398.4a, BioLegend). Goat anti-hamster IgG (20 µg/mL, SouthernBiotech) was added for crosslinking and cells were immediately incubated for the indicated timepoints in a 37ºC waterbath. Restimulation was stopped using ice-cold STOP buffer (PBS, 10% FBS, 1 mM Na_3VO_4, 1 mM EDTA). Cytoplasmic and nuclear fractions of restimulated T cells were obtained using the NE-PER kit (ThermoFisher) according to the manufacturer's instructions. Lysates were boiled in Laemmli buffer and samples were run on SDS-PAGE gels. Proteins were transferred to Amersham nitrocellulose membranes (GE Healthcare). Membranes were blocked using 3% BSA in TBS-T. The following antibodies were used for detection according to manufacturer's instructions: anti-NFAT2 (D15F1, Cell Signaling Technology), anti-α-tubulin (2144, New England Biolabs), anti-Histone H3 (4499, New England Biolabs) and anti-mouse IgG-HRP (Santa Cruz Biotechnology). Detection was performed using Amersham ECL prime kits (GE healthcare) and images were captured using a ChemiDoc imaging system (Bio-Rad). Band quantification was performed using ImageJ and normalized to loading controls.

Statistical analysis

Data is presented as mean ± SEM unless specified otherwise. For single comparisons, statistical significance was judged using two-tailed Student *t*-tests. For multiple comparisons, the Holm-Sidak *t*-test was used. For single-cell gene expression comparisons between clusters, the Wilcoxon signed-rank test was used. R^2 values were obtained by linear regression. Statistical significance was judged based on *p* values and is indicated as follows: $*p<0.05$, $**p<0.01$, $***p<0.001$. Analysis was performed using Prism 7 (GraphPad software).

References

1 Crotty, S. Follicular helper CD4 T cells (TFH). *Annu. Rev. Immunol* **29**, 621-663 (2011).

2 Victora, G. D. & Nussenzweig, M. C. Germinal centers. *Annu. Rev. Immunol* **30**, 429-457, doi:10.1146 (2012).

3 Fazilleau, N., Mark, L., Heyzer-Williams, L. J. & Heyzer-Williams, M. G. Follicular helper T cells: lineage and location. *Immunity* **20;30**, 324-335 (2009).

4 Nurieva, R. I. *et al.* Bcl6 mediates the development of T follicular helper cells. *Science* **325**, 1001-1005 (2009).

5 Johnston, R. J. *et al.* Bcl6 and Blimp-1 are reciprocal and antagonistic regulators of T follicular helper cell differentiation. *Science* **325**, 1006-1010 (2009).

6 Yu, D. *et al.* The transcriptional repressor Bcl-6 directs T follicular helper cell lineage commitment. *Immunity* **31**, 457-468 (2009).

7 Reinhardt, R. L., Liang, H. E. & Locksley, R. M. Cytokine-secreting follicular T cells shape the antibody repertoire. *Nat. Immunol* **10**, 385-393 (2009).

8 Bryant, V. L. *et al.* Cytokine-mediated regulation of human B cell differentiation into Ig-secreting cells: predominant role of IL-21 produced by CXCR5+ T follicular helper cells. *J Immunol* **179**, 8180-8190, doi:10.4049/jimmunol.179.12.8180 (2007).

9 Crotty, S. T Follicular Helper Cell Differentiation, Function, and Roles in Disease. *Immunity* **41**, 529-542 (2014).

10 Linterman, M. A. *et al.* Follicular helper T cells are required for systemic autoimmunity. *J. Exp. Med* **206**, 561-576 (2009).

11 Chung, Y. *et al.* Follicular regulatory T cells expressing Foxp3 and Bcl-6 suppress germinal center reactions. *Nat. Med* **17**, 983-988 (2011).

12 Linterman, M. A. *et al.* Foxp3+ follicular regulatory T cells control the germinal center response. *Nat. Med* **17**, 975-982 (2011).

13 Wollenberg, I. *et al.* Regulation of the germinal center reaction by Foxp3+ follicular regulatory T cells. *J Immunol* **187**, 4553-4560, doi:10.4049/jimmunol.1101328 (2011).

14 Sayin, I. *et al.* Spatial distribution and function of T follicular regulatory cells in human lymph nodes. *J Exp Med* **215**, 1531-1542, doi:10.1084/jem.20171940 (2018).

15 Vaeth, M. *et al.* Follicular regulatory T cells control humoral autoimmunity via NFAT2-regulated CXCR5 expression. *J Exp Med* **211**, 545-561, doi:10.1084/jem.20130604 (2014).

16 Oestreich, K. J., Mohn, S. E. & Weinmann, A. S. Molecular mechanisms that control the expression and activity of Bcl-6 in TH1 cells to regulate flexibility with a TFH-like gene profile. *Nat. Immunol* **13**, 405-411 (2012).

17 Shaffer, A. L. *et al.* Blimp-1 orchestrates plasma cell differentiation by extinguishing the mature B cell gene expression program. *Immunity* **17**, 51-62, doi:10.1016/s1074-7613(02)00335-7 (2002).

18 Hou, S. *et al.* FoxP3 and Ezh2 regulate Tfr cell suppressive function and transcriptional program. *J Exp Med* **216**, 605-620, doi:10.1084/jem.20181134 (2019).

19 Wu, H. *et al.* Follicular regulatory T cells repress cytokine production by follicular helper T cells and optimize IgG responses in mice. *Eur J Immunol* **46**, 1152-1161, doi:10.1002/eji.201546094 (2016).

20 Maceiras, A. R. *et al.* T follicular helper and T follicular regulatory cells have different TCR specificity. *Nat Commun* **8**, 15067, doi:10.1038/ncomms15067 (2017).

21 Aloulou, M. *et al.* Follicular regulatory T cells can be specific for the immunizing antigen and derive from naive T cells. *Nat Commun* **7**, 10579, doi:10.1038/ncomms10579 (2016).

22 Botta, D. *et al.* Dynamic regulation of T follicular regulatory cell responses by interleukin 2 during influenza infection. *Nat Immunol* **18**, 1249-1260, doi:10.1038/ni.3837 (2017).
23 Hao, H. *et al.* Conversion of T Follicular Helper Cells to T Follicular Regulatory Cells by Interleukin-2 Through Transcriptional Regulation in Systemic Lupus Erythematosus. *Arthritis Rheumatol* **73**, 132-142, doi:10.1002/art.41457 (2021).
24 Jacobsen, J. T. *et al.* Expression of Foxp3 by T follicular helper cells in end-stage germinal centers. *Science* **373**, doi:10.1126/science.abe5146 (2021).
25 Sage, P. T., Alvarez, D., Godec, J., von Andrian, U. H. & Sharpe, A. H. Circulating T follicular regulatory and helper cells have memory-like properties. *J. Clin. Invest*, 76861 (2014).
26 Sage, P. T., Francisco, L. M., Carman, C. V. & Sharpe, A. H. The receptor PD-1 controls follicular regulatory T cells in the lymph nodes and blood. *Nat Immunol* **14**, 152-161, doi:10.1038/ni.2496 (2013).
27 Clement, R. L. *et al.* Follicular regulatory T cells control humoral and allergic immunity by restraining early B cell responses. *Nat Immunol* **20**, 1360-1371, doi:10.1038/s41590-019-0472-4 (2019).
28 Fu, W. *et al.* Deficiency in T follicular regulatory cells promotes autoimmunity. *J Exp Med*, doi:10.1084/jem.20170901 (2018).
29 Xie, M. M. & Dent, A. L. Unexpected Help: Follicular Regulatory T Cells in the Germinal Center. *Front Immunol* **9**, 1536, doi:10.3389/fimmu.2018.01536 (2018).
30 Laidlaw, B. J. *et al.* Interleukin-10 from CD4(+) follicular regulatory T cells promotes the germinal center response. *Sci Immunol* **2**, doi:10.1126/sciimmunol.aan4767 (2017).
31 Sage, P. T. & Sharpe, A. H. The multifaceted functions of follicular regulatory T cells. *Curr Opin Immunol* **67**, 68-74, doi:10.1016/j.coi.2020.10.009 (2020).
32 Hutloff, A. *et al.* ICOS is an inducible T-cell co-stimulator structurally and functionally related to CD28. *Nature* **397**, 263-266 (1999).
33 Bossaller, L. *et al.* ICOS deficiency is associated with a severe reduction of CXCR5+CD4 germinal center Th cells. *J. Immunol* **177**, 4927-4932 (2006).
34 Leavenworth, J. W., Verbinnen, B., Yin, J., Huang, H. & Cantor, H. A p85alpha-osteopontin axis couples the receptor ICOS to sustained Bcl-6 expression by follicular helper and regulatory T cells. *Nat Immunol* **16**, 96-106, doi:10.1038/ni.3050 (2015).
35 Gigoux, M. *et al.* Inducible costimulator promotes helper T-cell differentiation through phosphoinositide 3-kinase. *Proc. Natl. Acad. Sci. U. S. A* **106**, 20371-20376 (2009).
36 Tafuri, A. *et al.* ICOS is essential for effective T-helper-cell responses. *Nature* **409**, 105-109 (2001).
37 McAdam, A. J. *et al.* ICOS is critical for CD40-mediated antibody class switching. *Nature* **409**, 102-105 (2001).
38 Dong, C. *et al.* ICOS co-stimulatory receptor is essential for T-cell activation and function. *Nature* **409**, 97-101 (2001).
39 Grimbacher, B. *et al.* Homozygous loss of ICOS is associated with adult-onset common variable immunodeficiency. *Nat Immunol* **4**, 261-268 (2003).
40 Takahashi, N. *et al.* Impaired CD4 and CD8 effector function and decreased memory T cell populations in ICOS-deficient patients. *J. Immunol* **182**, 5515-5527 (2009).
41 Warnatz, K. *et al.* Human ICOS deficiency abrogates the germinal center reaction and provides a monogenic model for common variable immunodeficiency. *Blood* **107**, 3045-3052 (2006).
42 Zhang, M. *et al.* Inducible T-Cell Co-Stimulator Impacts Chronic Graft-Versus-Host Disease by Regulating Both Pathogenic and Regulatory T Cells. *Front Immunol* **9**, 1461, doi:10.3389/fimmu.2018.01461 (2018).

43 Allie, S. R. *et al.* The establishment of resident memory B cells in the lung requires local antigen encounter. *Nat Immunol* **20**, 97-108, doi:10.1038/s41590-018-0260-6 (2019).
44 Lam, J. H. & Baumgarth, N. The Multifaceted B Cell Response to Influenza Virus. *J Immunol* **202**, 351-359, doi:10.4049/jimmunol.1801208 (2019).
45 Castro, C. & Gourley, M. Diagnostic testing and interpretation of tests for autoimmunity. *J Allergy Clin Immunol* **125**, S238-247, doi:10.1016/j.jaci.2009.09.041 (2010).
46 Wing, J. B. *et al.* A distinct subpopulation of CD25(-) T-follicular regulatory cells localizes in the germinal centers. *Proc Natl Acad Sci U S A* **114**, E6400-E6409, doi:10.1073/pnas.1705551114 (2017).
47 McIntyre, T. M. *et al.* Transforming growth factor beta 1 selectivity stimulates immunoglobulin G2b secretion by lipopolysaccharide-activated murine B cells. *J Exp Med* **177**, 1031-1037, doi:10.1084/jem.177.4.1031 (1993).
48 Weber, J. P. *et al.* ICOS maintains the T follicular helper cell phenotype by down-regulating Kruppel-like factor 2. *J Exp Med* **212**, 217-233, doi:10.1084/jem.20141432 (2015).
49 Lee, J. Y. *et al.* The transcription factor KLF2 restrains CD4(+) T follicular helper cell differentiation. *Immunity* **42**, 252-264, doi:10.1016/j.immuni.2015.01.013 (2015).
50 Hogan, P. G., Chen, L., Nardone, J. & Rao, A. Transcriptional regulation by calcium, calcineurin, and NFAT. *Genes Dev* **17**, 2205-2232, doi:10.1101/gad.1102703 (2003).
51 Leconte, J., Bagherzadeh Yazdchi, S., Panneton, V. & Suh, W. K. Inducible costimulator (ICOS) potentiates TCR-induced calcium flux by augmenting PLCgamma1 activation and actin remodeling. *Mol Immunol* **79**, 38-46, doi:10.1016/j.molimm.2016.09.022 (2016).
52 Bettini, M. L. & Vignali, D. A. Development of thymically derived natural regulatory T cells. *Ann N Y Acad Sci* **1183**, 1-12, doi:10.1111/j.1749-6632.2009.05129.x (2010).
53 Beals, C. R., Sheridan, C. M., Turck, C. W., Gardner, P. & Crabtree, G. R. Nuclear export of NF-ATc enhanced by glycogen synthase kinase-3. *Science* **275**, 1930-1934, doi:10.1126/science.275.5308.1930 (1997).
54 Yoeli-Lerner, M., Chin, Y. R., Hansen, C. K. & Toker, A. Akt/protein kinase b and glycogen synthase kinase-3beta signaling pathway regulates cell migration through the NFAT1 transcription factor. *Mol Cancer Res* **7**, 425-432, doi:10.1158/1541-7786.MCR-08-0342 (2009).
55 Parry, R. V., Rumbley, C. A., Vandenberghe, L. H., June, C. H. & Riley, J. L. CD28 and inducible costimulatory protein Src homology 2 binding domains show distinct regulation of phosphatidylinositol 3-kinase, Bcl-x(L), and IL-2 expression in primary human CD4 T lymphocytes. *J Immunol* **171**, 166-174 (2003).
56 Arimura, Y. *et al.* A co-stimulatory molecule on activated T cells, H4/ICOS, delivers specific signals in T(h) cells and regulates their responses. *Int Immunol* **14**, 555-566 (2002).
57 Liu, D. *et al.* T-B-cell entanglement and ICOSL-driven feed-forward regulation of germinal centre reaction. *Nature* **517**, 214-218, doi:10.1038/nature13803 (2015).
58 Xie, M. M. *et al.* Follicular regulatory T cells inhibit the development of granzyme B-expressing follicular helper T cells. *JCI Insight* **4**, doi:10.1172/jci.insight.128076 (2019).
59 Xie, M. M. *et al.* T follicular regulatory cells and IL-10 promote food antigen-specific IgE. *J Clin Invest* **130**, 3820-3832, doi:10.1172/JCI132249 (2020).
60 Li, Y. *et al.* Bcl6 Preserves the Suppressive Function of Regulatory T Cells During Tumorigenesis. *Front Immunol* **11**, 806, doi:10.3389/fimmu.2020.00806 (2020).
61 Sawant, D. V. *et al.* Bcl6 controls the Th2 inflammatory activity of regulatory T cells by repressing Gata3 function. *J Immunol* **189**, 4759-4769, doi:10.4049/jimmunol.1201794 (2012).
62 Sawant, D. V. *et al.* The transcriptional repressor Bcl6 controls the stability of regulatory T cells by intrinsic and extrinsic pathways. *Immunology* **145**, 11-23, doi:10.1111/imm.12393 (2015).

63 Busse, M., Krech, M., Meyer-Bahlburg, A., Hennig, C. & Hansen, G. ICOS mediates the generation and function of CD4+CD25+Foxp3+ regulatory T cells conveying respiratory tolerance. *J Immunol* **189**, 1975-1982, doi:10.4049/jimmunol.1103581 (2012).
64 Kornete, M., Sgouroudis, E. & Piccirillo, C. A. ICOS-dependent homeostasis and function of Foxp3+ regulatory T cells in islets of nonobese diabetic mice. *J Immunol* **188**, 1064-1074, doi:10.4049/jimmunol.1101303 (2012).
65 Rubtsov, Y. P. *et al.* Regulatory T cell-derived interleukin-10 limits inflammation at environmental interfaces. *Immunity* **28**, 546-558, doi:10.1016/j.immuni.2008.02.017 (2008).
66 Rubtsov, Y. P. *et al.* Stability of the regulatory T cell lineage in vivo. *Science* **329**, 1667-1671, doi:10.1126/science.1191996 (2010).
67 Panneton, V., Bagherzadeh Yazdchi, S., Witalis, M., Chang, J. & Suh, W.-K. ICOS Signaling Controls Induction and Maintenance of Collagen-Induced Arthritis. *The Journal of Immunology* **200**, 3067 (2018).
68 Stuart, T. *et al.* Comprehensive Integration of Single-Cell Data. *Cell* **177**, 1888-1902 e1821, doi:10.1016/j.cell.2019.05.031 (2019).
69 Waltman, L., Jan van Eck, N. . A smart local moving algorithm for large-scale modularity-based community detection. *arXiv* **1308.6604** (2013).
70 McInnes, L., Healy, J., Melville, J. UMAP: Uniform Manifold Approximation and Projection for Dimension Reduction. *ArXiv* **1802.03426** (2020).
71 Trapnell, C. *et al.* The dynamics and regulators of cell fate decisions are revealed by pseudotemporal ordering of single cells. *Nat Biotechnol* **32**, 381-386, doi:10.1038/nbt.2859 (2014).
72 Angerer, P. *et al.* destiny: diffusion maps for large-scale single-cell data in R. *Bioinformatics* **32**, 1241-1243, doi:10.1093/bioinformatics/btv715 (2016).
73 Mi, H. *et al.* PANTHER version 16: a revised family classification, tree-based classification tool, enhancer regions and extensive API. *Nucleic Acids Res* **49**, D394-D403, doi:10.1093/nar/gkaa1106 (2021).
74 Mognol, G. P., Carneiro, F. R., Robbs, B. K., Faget, D. V. & Viola, J. P. Cell cycle and apoptosis regulation by NFAT transcription factors: new roles for an old player. *Cell Death Dis* **7**, e2199, doi:10.1038/cddis.2016.97 (2016).
75 Hermann-Kleiter, N. & Baier, G. NFAT pulls the strings during CD4+ T helper cell effector functions. *Blood* **115**, 2989-2997, doi:10.1182/blood-2009-10-233585 (2010).

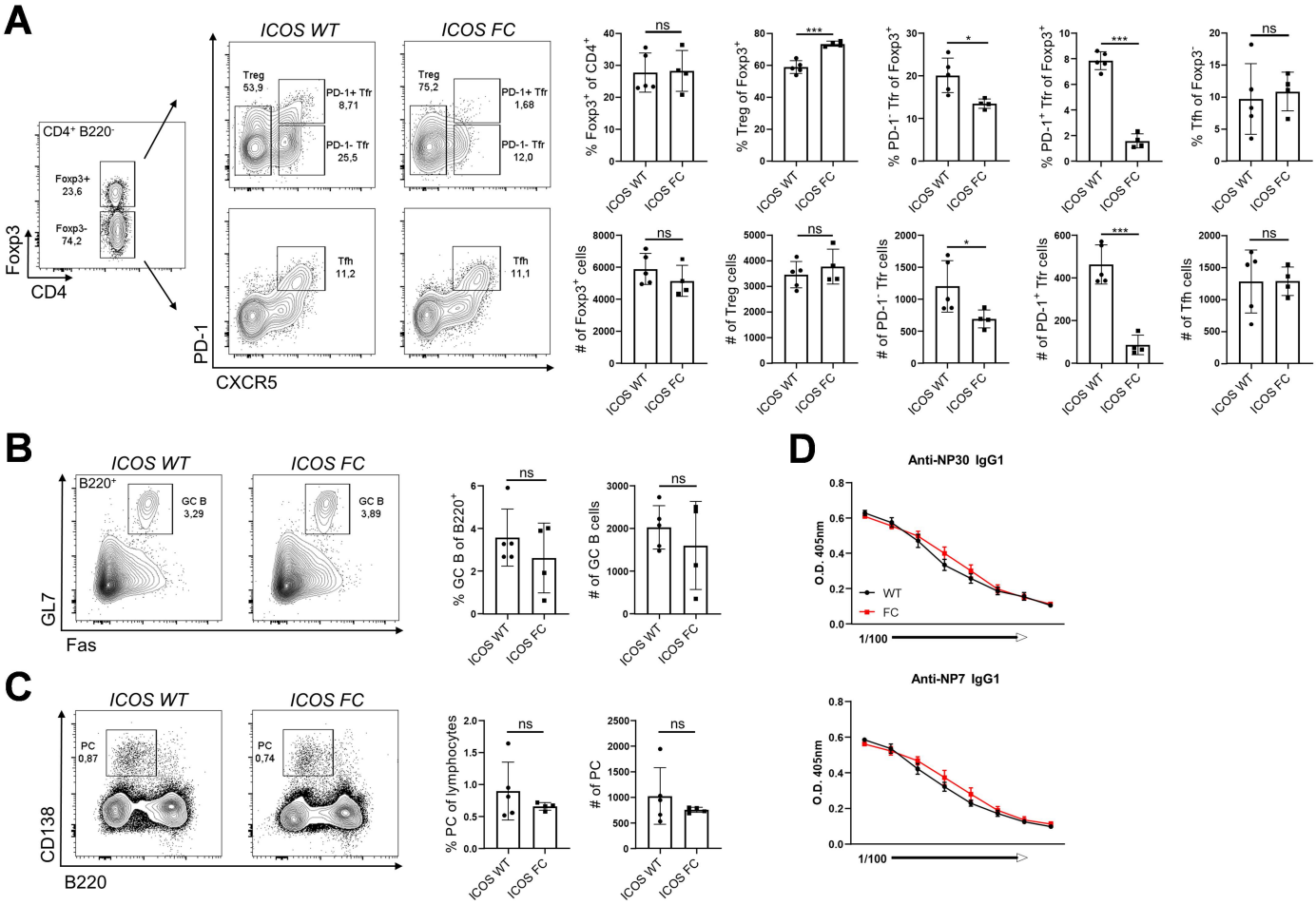
A
ICOS WT
ICOS FC
CD4+ B220-
Foxp3+ 23,6
Foxp3- 74,2
Foxp3
CD4
Treg 53,9
PD-1+ Tfr 8,71
PD-1- Tfr 25,5
Treg 75,2
PD-1+ Tfr 1,68
PD-1- Tfr 12,0
Tfh 11,2
Tfh 11,1
PD-1
CXCR5
% Foxp3+ of CD4+
% Treg of Foxp3+
% PD-1- Tfr of Foxp3+
% PD-1+ Tfr of Foxp3+
% Tfh of Foxp3-
# of Foxp3+ cells
# of Treg cells
# of PD-1- Tfr cells
# of PD-1+ Tfr cells
# of Tfh cells
ICOS WT
ICOS FC
ns
*
***
B
B220+
GC B 3,29
GC B 3,89
GL7
Fas
% GC B of B220+
# of GC B cells
C
PC 0,87
PC 0,74
CD138
B220
% PC of lymphocytes
# of PC
D
Anti-NP30 IgG1
Anti-NP7 IgG1
O.D. 405nm
WT
FC
1/100

Figure 1

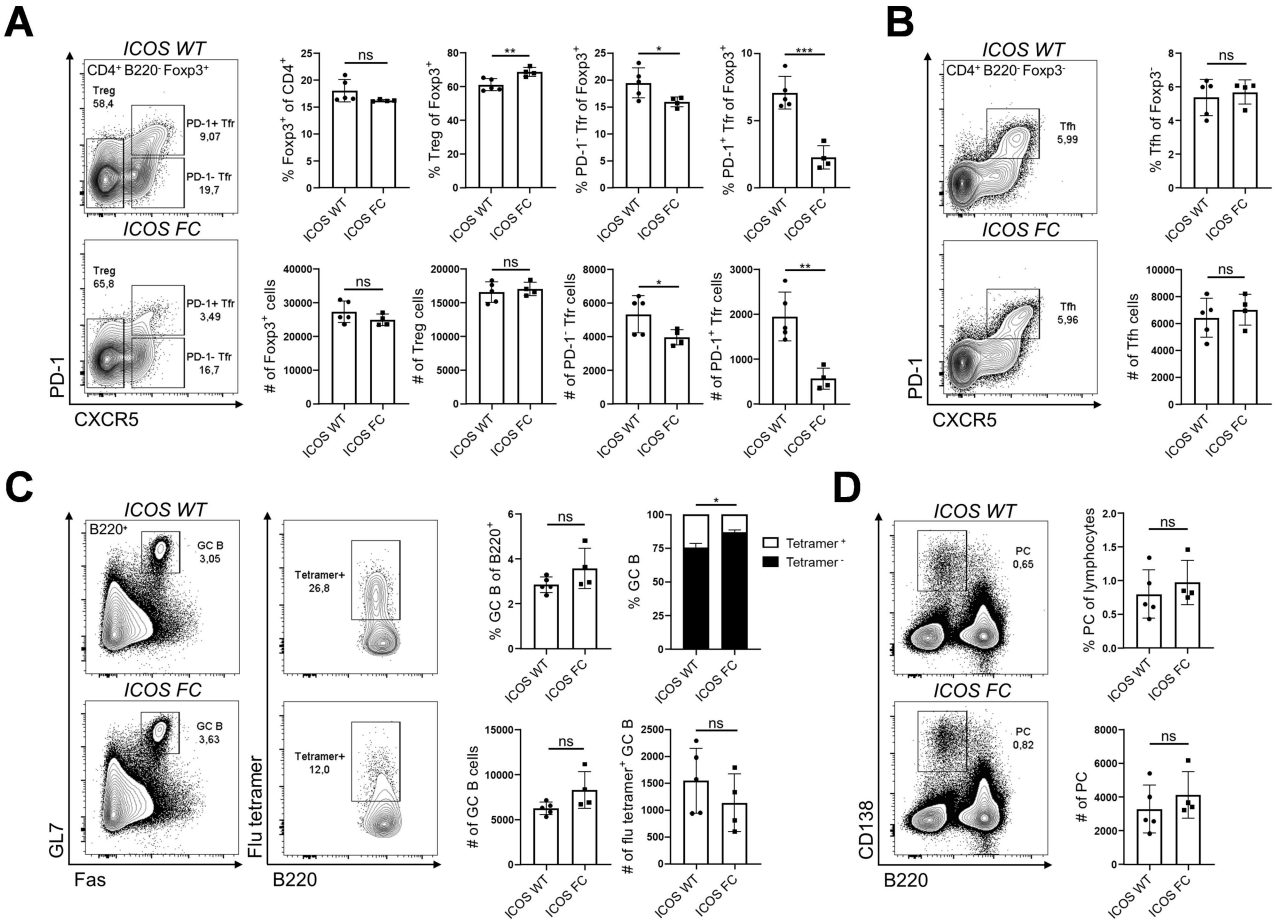
A
ICOS WT
CD4+ B220- Foxp3+
Treg 58,4
PD-1+ Tfr 9,07
PD-1- Tfr 19,7
ICOS FC
Treg 65,8
PD-1+ Tfr 3,49
PD-1- Tfr 16,7
PD-1
CXCR5
% Foxp3+ of CD4+
% Treg of Foxp3+
% PD-1- Tfr of Foxp3+
% PD-1+ Tfr of Foxp3+
# of Foxp3+ cells
# of Treg cells
# of PD-1- Tfr cells
# of PD-1+ Tfr cells
ICOS WT
ICOS FC
ns
**
*
***
B
CD4+ B220- Foxp3-
Tfh 5,99
Tfh 5,96
% Tfh of Foxp3-
# of Tfh cells
C
B220+
GC B 3,05
GC B 3,63
GL7
Fas
Tetramer+ 26,8
Tetramer+ 12,0
Flu tetramer
B220
% GC B of B220+
% GC B
Tetramer+
Tetramer-
# of GC B cells
# of flu tetramer+ GC B
D
PC 0,65
PC 0,82
CD138
% PC of lymphocytes
# of PC

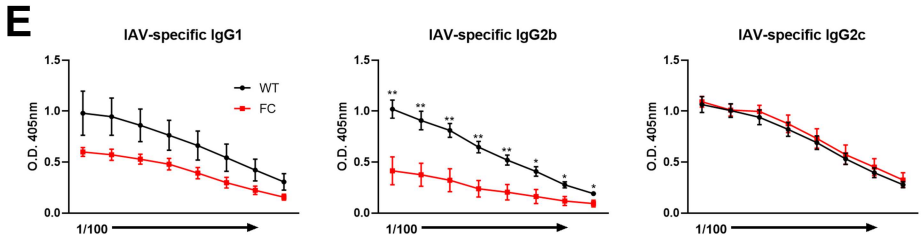
E
IAV-specific IgG1
IAV-specific IgG2b
IAV-specific IgG2c
WT
FC
O.D. 405nm
1/100

Figure 2

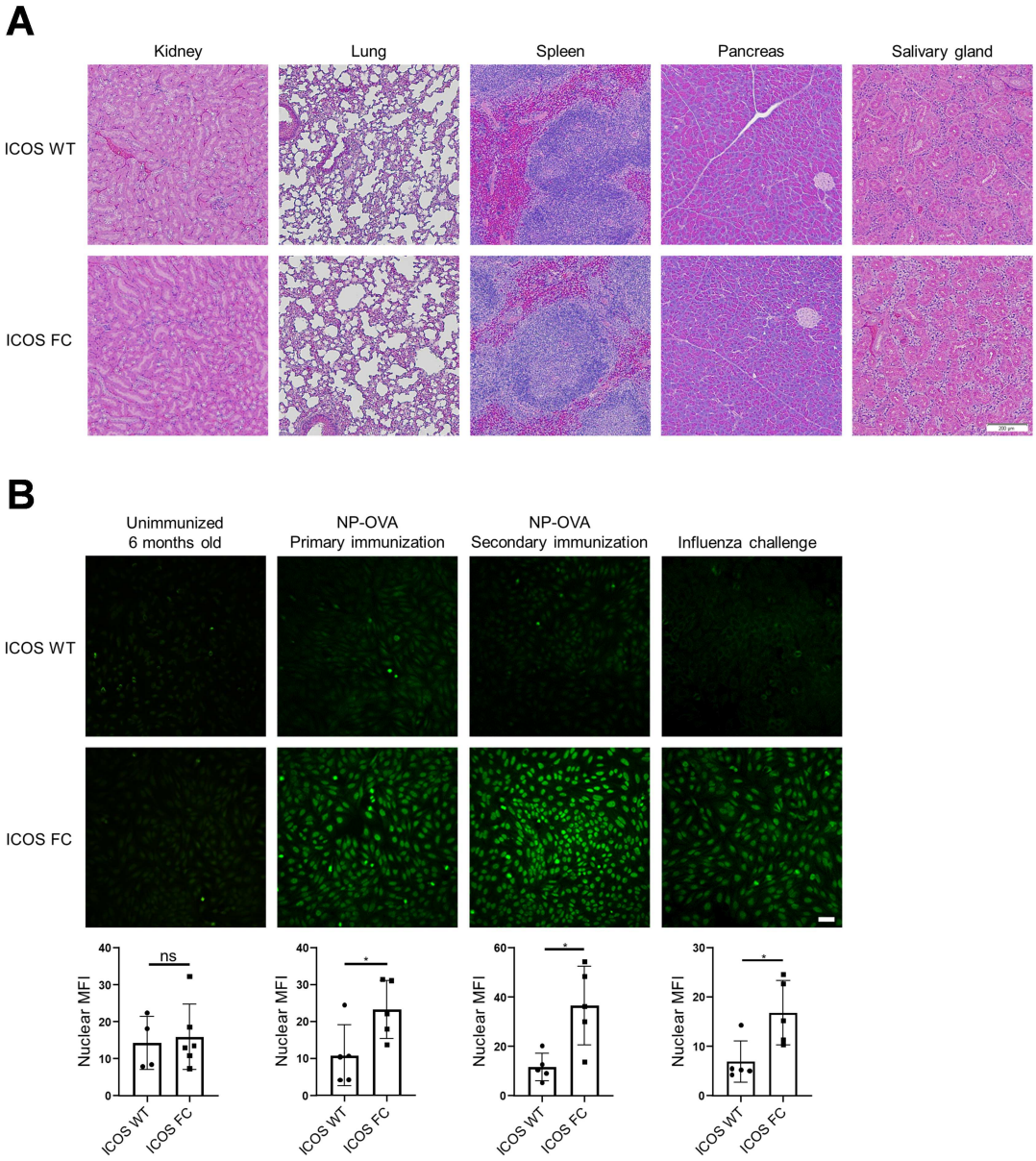
A
Kidney
Lung
Spleen
Pancreas
Salivary gland
ICOS WT
ICOS FC
B
Unimmunized
6 months old
NP-OVA
Primary immunization
NP-OVA
Secondary immunization
Influenza challenge
ICOS WT
ICOS FC
Nuclear MFI
ns
*
ICOS WT
ICOS FC

Figure 3

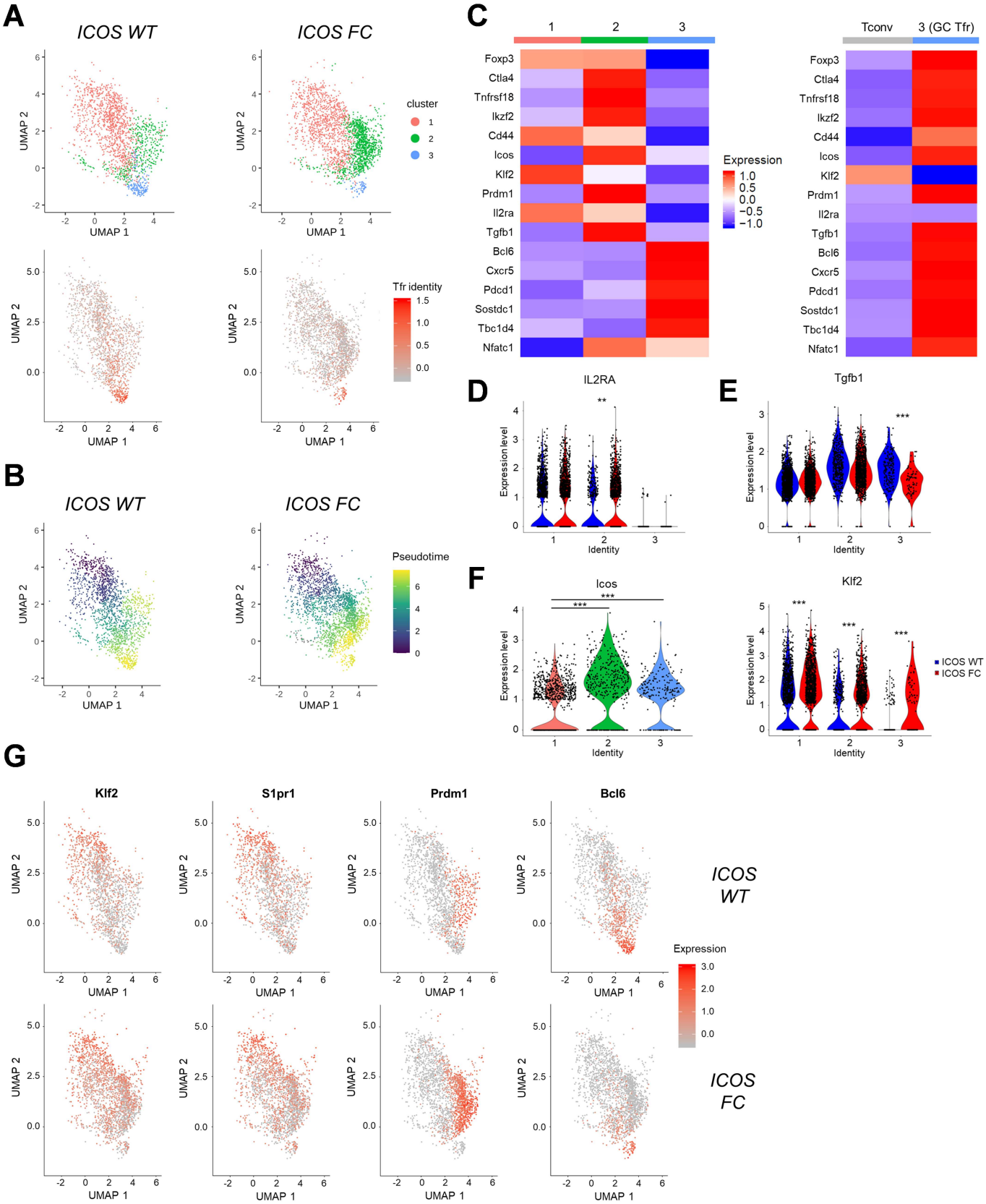
A
ICOS WT
ICOS FC
UMAP 1
UMAP 2
cluster
1
2
3
Tfr identity
B
Pseudotime
C
Foxp3
Ctla4
Tnfrsf18
Ikzf2
Cd44
Icos
Klf2
Prdm1
Il2ra
Tgfb1
Bcl6
Cxcr5
Pdcd1
Sostdc1
Tbc1d4
Nfatc1
Tconv
3 (GC Tfr)
Expression
D
IL2RA
Expression level
Identity
E
Tgfb1
F
Icos
Klf2
ICOS WT
ICOS FC
G
Klf2
S1pr1
Prdm1
Bcl6
ICOS WT
ICOS FC

Figure 4

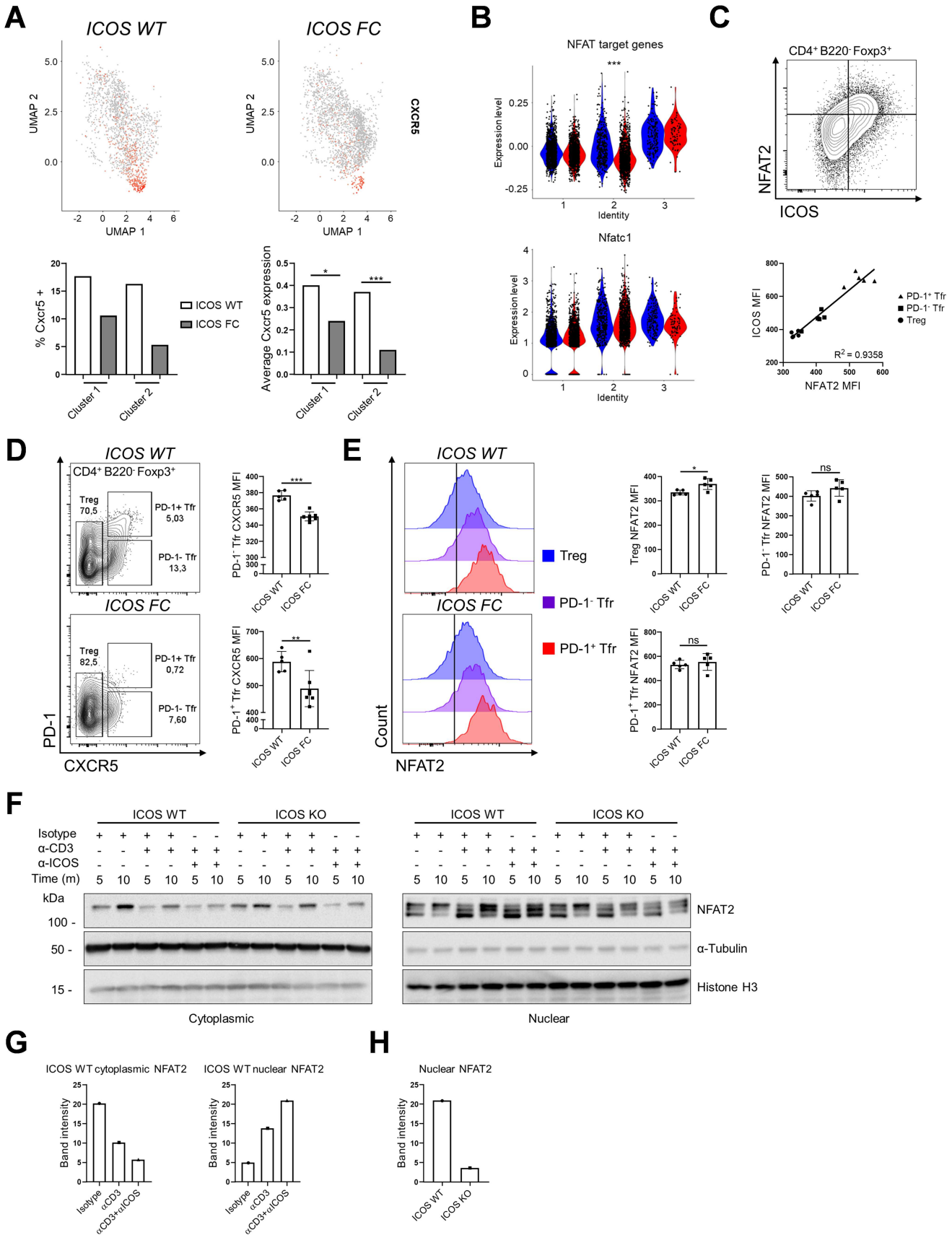
A
ICOS WT
ICOS FC
UMAP 2
UMAP 1
CXCR5
% Cxcr5 +
ICOS WT
ICOS FC
Cluster 1
Cluster 2
Average Cxcr5 expression
B
NFAT target genes
Expression level
Identity
Nfatc1
C
CD4+ B220- Foxp3+
NFAT2
ICOS
ICOS MFI
NFAT2 MFI
PD-1+ Tfr
PD-1- Tfr
Treg
R2 = 0.9358
D
ICOS WT
ICOS FC
CD4+ B220- Foxp3+
Treg 70,5
PD-1+ Tfr 5,03
PD-1- Tfr 13,3
Treg 82,5
PD-1+ Tfr 0,72
PD-1- Tfr 7,60
PD-1
CXCR5
PD-1- Tfr CXCR5 MFI
PD-1+ Tfr CXCR5 MFI
E
Treg
PD-1- Tfr
PD-1+ Tfr
Count
NFAT2
Treg NFAT2 MFI
PD-1- Tfr NFAT2 MFI
PD-1+ Tfr NFAT2 MFI
ns
F
ICOS WT
ICOS KO
Isotype
α-CD3
α-ICOS
Time (m)
kDa
100 -
50 -
15 -
NFAT2
α-Tubulin
Histone H3
Cytoplasmic
Nuclear
G
ICOS WT cytoplasmic NFAT2
ICOS WT nuclear NFAT2
Band intensity
Isotype
αCD3
αCD3+αICOS
H
Nuclear NFAT2
ICOS WT
ICOS KO

Figure 5

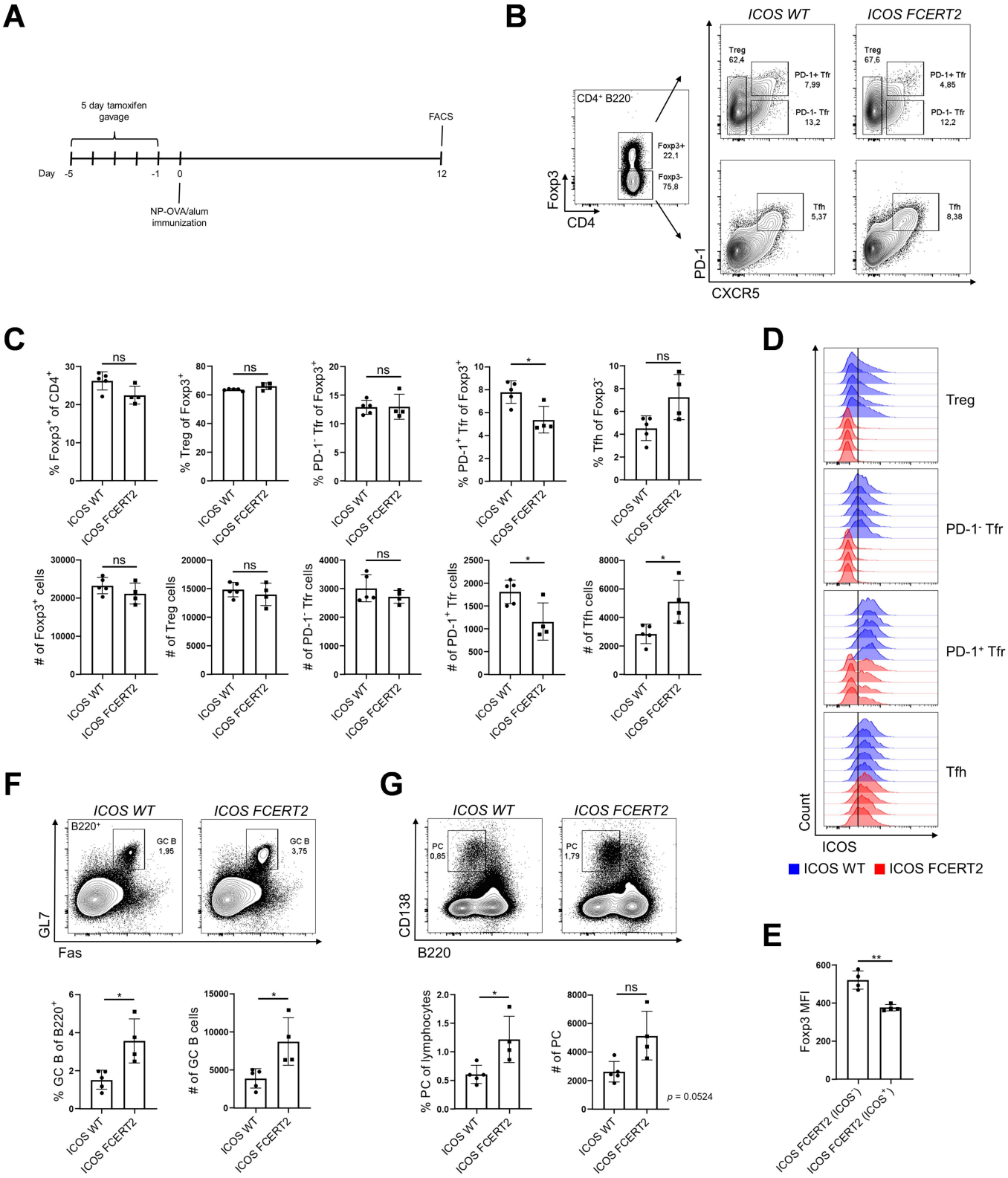
A
5 day tamoxifen gavage
FACS
Day -5
-1
0
12
NP-OVA/alum immunization
B
ICOS WT
ICOS FCERT2
CD4+ B220-
Foxp3+ 22,1
Foxp3- 75,8
Foxp3
CD4
Treg 62,4
PD-1+ Tfr 7,99
PD-1- Tfr 13,2
Treg 67,6
PD-1+ Tfr 4,85
PD-1- Tfr 12,2
Tfh 5,37
Tfh 8,38
PD-1
CXCR5
C
% Foxp3+ of CD4+
% Treg of Foxp3+
% PD-1- Tfr of Foxp3+
% PD-1+ Tfr of Foxp3+
% Tfh of Foxp3-
# of Foxp3+ cells
# of Treg cells
# of PD-1- Tfr cells
# of PD-1+ Tfr cells
# of Tfh cells
ns
*
ICOS WT
ICOS FCERT2
D
Treg
PD-1- Tfr
PD-1+ Tfr
Tfh
Count
ICOS
ICOS WT
ICOS FCERT2
E
Foxp3 MFI
**
ICOS FCERT2 (ICOS-)
ICOS FCERT2 (ICOS+)
F
ICOS WT
ICOS FCERT2
B220+
GC B 1,95
GC B 3,75
GL7
Fas
% GC B of B220+
# of GC B cells
G
PC 0,85
PC 1,79
CD138
B220
% PC of lymphocytes
# of PC
p = 0.0524

Figure 6

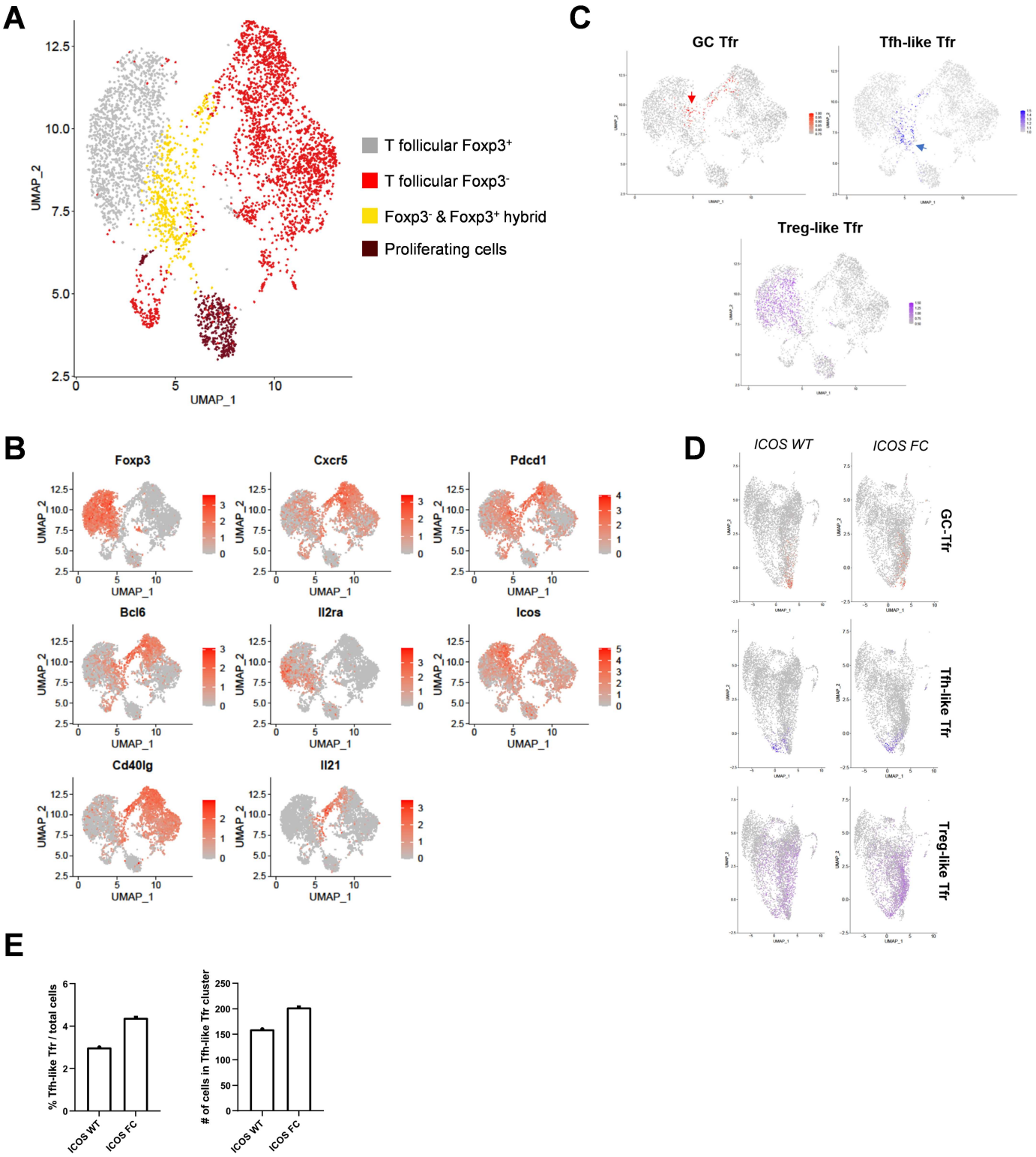
A
UMAP_2
UMAP_1
T follicular Foxp3+
T follicular Foxp3-
Foxp3- & Foxp3+ hybrid
Proliferating cells
C
GC Tfr
Tfh-like Tfr
Treg-like Tfr
B
Foxp3
Cxcr5
Pdcd1
Bcl6
Il2ra
Icos
Cd40lg
Il21
D
ICOS WT
ICOS FC
GC-Tfr
Tfh-like Tfr
Treg-like Tfr
E
% Tfh-like Tfr / total cells
# of cells in Tfh-like Tfr cluster
ICOS WT
ICOS FC

Figure 7